Pulsing to Improve Bubble Column Performance: I. Low Gas Rates

F. Carl Knopf, Jia Ma, and Richard G. Rice
Dept. of Chemical Engineering, Louisiana State University, Baton Rouge, LA 70803

Dimitris Nikitopoulos
Dept. of Mechanical Engineering, Louisiana State University, Baton Rouge, LA 70803

DOI 10.1002/aic.10698
Published online November 1, 2005 in Wiley InterScience (www.interscience.wiley.com).

The liquid phase of a batch bubble column was subjected to low-amplitude pulsations at modest frequencies (range 0–30 Hz). At low gas rates (up to 5 mL/s) using a single-injector tube we found that substantial bubble breakage occurred at frequencies < 30 Hz. At the low flow rates examined, enhanced bubble breakup occurred mainly as a result of two-phase flow developing within the injector tube. External sinusoidal pulsation caused high-velocity water ingestion (suck-back) and expulsion from the injector. This suck-back action caused intense fragmentation of gas slugs within the injector, often into many very small bubbles, as high-speed imaging showed. Mass transfer coefficients were measured as a function of pulsation frequency and driver amplitudes at several air flow rates, demonstrating the benefits of this type of pulsed bubble column. A simple dynamic mechanical model of the pulsed liquid column predicted resonance, which depended on membrane thickness of the driving piston. © 2005 American Institute of Chemical Engineers
AIChE J, 52: 1103–1115, 2006
Keywords: oscillation, bubble columns, moss transfer

Introduction

Bubble column reactors (BCRs) are well known to produce effective gas–liquid contact. These reactors have few moving parts and low operational costs. Of key importance in bubble column operation is the generation of small bubbles to promote a large interfacial area between gas and liquid. However, it is difficult to forecast or predict the behavior of BCRs because of the highly chaotic nature of bubble swarms. Even the method of gas injection (single orifice, perforated plate, perforated rubber sheet, or sintered disk) has a measurable effect on performance. The process of bubble breakage and coalescence is still not well understood, and the mechanism for the onset of liquid circulation is a major unknown.

This project grew from efforts to use active forcing to improve spray combustion efficiency.[1] Active forcing involves the modulation or pulsing of the fuel streams and air streams to a combustor, at the acoustic resonant frequency of the combustor. The basic concept is that acoustic modulation of the primary air stream strengthens the coherent vortices of the flow field. The injection of the fuel droplets at the onset of vortex roll up provides better mixing between the droplets and the airstream, leading to improved combustion efficiency. We seek to extend the concept of active forcing to other chemical reacting systems, notably bubble column reactors.

In 1964, Bretsznajder and Pasiuk[2] noted that "intensification of (liquid–liquid) mass transfer processes by the method of pulsation already has a tradition of almost 30 years. . . . When we took it up, in 1959 (see Bretsznajder et al.[3]), the study of the influence of pulsating motion on mass diffusion in a gas–liquid system, we found no work on this subject in the available literature."

Over the past 40 years, forcing by oscillations to improve mass transfer in bubble columns has been extensively stud-

Correspondence concerning this article should be addressed to F. C. Knopf at knopf@lsu.edu or R. G. Rice at dickrice@wwgap.net.

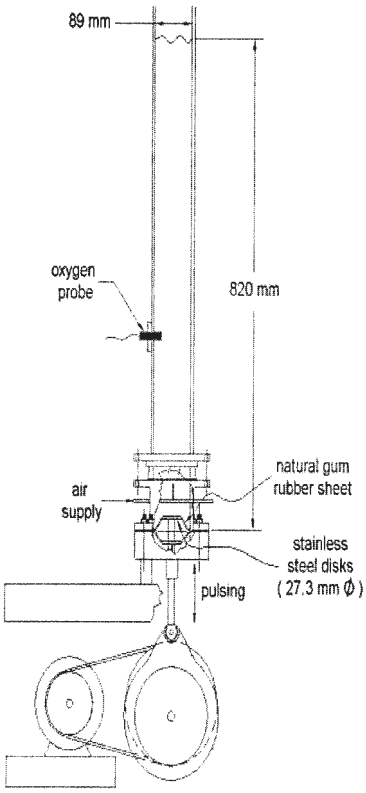

Figure 1. Pulsed bubble column reactor.

ied[4-9] and recently Krishna and coworkers[10,11] have rejuvenated interest. Early work focused on column-proper effects including resonant bubble breakup and bubble rise times to explain transport enhancements under vibration.[12-15] For low gas flow rates, attention is now also being focused on bubble formation at the orifice under forcing conditions.[16-21]

For low gas rates, pulsing (forcing) causes a complex set of processes for bubble breakage, which involves liquid backflow in the gas injector and the impact of high momentum liquid slugs on bubbles near the injector tip. The objective of the work presented here is to investigate this observation in greater detail, including the use of both a high-speed camera and simple mass transfer experiments to assess the enhancement achieved, relative to the unforced case. Results are explained by considering the resonant behavior of the sinusoidal forcing system.

A key to enhancements of mass transfer is the mode of forcing. Several possible equipment types are possible: total column vibration or fluid vibration by baffles or pistons. For the latter, one could use solid pistons (with attendant O-rings or piston rings as in a combustion engine) or, as in our case, use of a flexible piston. We elected to use a flexible piston of novel design as depicted in Figure 1. This flexible piston had no sealing problems and operated flawlessly. We now discuss the methods and procedures used to study forced enhancements.

Experimental

Equipment

The bubble column, constructed from Plexiglas®, is sealed at the base with a natural gum rubber sheet.[22] The column and ancillaries are shown in Figure 1. For all experiments, gas was introduced into the system through a single injector. Digital camera flow visualization experiments were made using a glass injector with an ID of 1.00 mm. All other experiments, including mass transfer measurements, used a stainless steel injector with an ID of 0.75 mm. For all experiments the injector height was held constant at 38 mm. Care was taken to ensure no burrs were present at the injector tip; a stereomicroscope was used for this purpose. The water used in the column was carefully distilled and deionized.

The natural gum rubber sheet at the base of the column is clamped between two stainless steel disks each 2.73 cm in diameter. These disks are directly coupled to an eccentric cam, which is driven by a 5-hp variable-speed motor. The motor speed is controlled by an Omron Sysdrive 3G 3JV compact inverter controller. The eccentric cam produces a sinusoidal oscillation in the disks/rubber sheet at the base of the column. The system is initially configured for operation from 0 to 30 Hz and amplitudes from 0 to 2.54 cm. By changing the pulley system, operation to 100 Hz is possible.

Gas was delivered to the column from an air cylinder with use of a pressure regulator. The pressure to the column was set to approximately 100 psig and a needle valve (Nupro PAT D) was used to control gas flow rate to the column. During the experiments the gas supply line used a 1.6 mm ID tube with a transition to the 1 mm ID glass tube that was used for gas injection inside the column during the visualization studies or a 0.75 mm stainless steel tube during other parts of the experiments. The needle valve placed in the 1.6 mm line before the transition to the smaller tube is a high-impedance element and the volume between this impedance and the injector tip was 1.38 mL.

Gas flow rates were set using a soap film meter at the column outlet. The flow rate was initially set without column pulsation because the flow rate did oscillate when pulsation was used. However, the average flow rate, as determined from the soap bubble meter, over an interval of a few seconds remained constant (even with pulsation). For high flow rate experiments the flow rate was checked using both a soap bubble meter and a totalizing dry test meter (Singer DTM-200). Average flow rates, as determined from the dry test meter, remained constant (even with pulsation).

Mass transfer coefficient measurements

A key aspect of the forcing technology is to assess potential enhancements, especially mass transfer. The generation of large bubble numbers, and consequently large surface area, using low energy input may allow agitator replacement with savings. To investigate improvements in mass transfer, we measured the mass transfer coefficient as a function of frequency at several air flow rates and amplitudes.

For mass transfer experiments, a dissolved oxygen probe (Cole Palmer Model 300mm) and signal conditioner (Model 01971-00) are placed in the bubble column, approximately 0.32 m above the injector. Gas bubbles do not directly influence the electrode. The column was initially purged of oxygen using nitrogen. After the dissolved oxygen content reached nearly 0 vol %, air flow was started.

The volumetric mass transfer coefficient was determined by measuring dissolved oxygen uptake in the bubble column as a

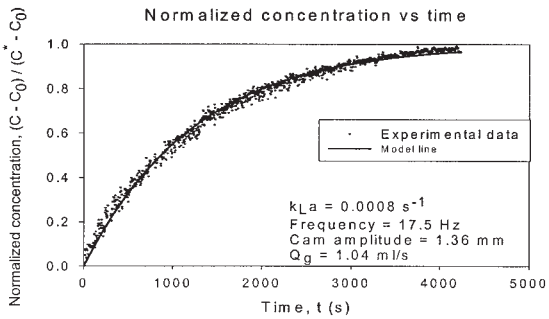

Figure 2. Normalized concentration of oxygen as a function of time together with fit for mass transfer coefficient.

f = 17.5 Hz, cam amplitude = 1.36 mm, Q_g = 1.04 mL/s (superficial nozzle gas velocity = 2.3 m/s).

function of time, assuming the vessel to be well mixed. Following Rice and Do,[23] the incremental rate expression for oxygen transfer (moles/time) into the liquid phase of a bubble column is given as the product of the volumetric mass transfer coefficient, multiplied by the linear composition driving force, and this times the incremental volume of the column, as

$$R = k_L a'(C^* - C) A_c \Delta z \tag{1}$$

Here, C^* and C represent the gas solubility and measured dissolved oxygen concentration (moles of solute/cm^3 liquid), respectively. A solute balance on the liquid phase simply states the rate of accumulation equals the rate of transfer:

$$A_c \Delta z(1 - \varepsilon) \frac{dC}{dt} = k_L a'(C^* - C) A_c \Delta z \tag{2}$$

where ε is the gas volume fraction or holdup and $(1 - \varepsilon)$ is the liquid holdup. Simplifying yields the following first-order equation:

$$(1 - \varepsilon) \frac{dC}{dt} = k_L a'(C^* - C) \tag{3}$$

Integration of Eq. 3 yields

$$C(t) = C^* - (C^* - C_0)\exp\left(-\frac{k_L a'}{(1 - \varepsilon)} t\right) \tag{4}$$

where C_0 (C at $t = 0$) is the initial oxygen concentration. Rearranging yields the dimensionless dissolved oxygen concentration as a function of time and mass-transfer coefficient, which for $C_0 = 0$ is

$$\frac{C(t)}{C^*} = 1 - \exp\left[-\frac{k_L a'}{(1 - \varepsilon)} t\right] \tag{5}$$

Combining the liquid fraction with a' yields

$$\frac{C(t)}{C^*} = 1 - \exp(-k_L a t) \tag{6}$$

where for perfectly spherical bubbles, $a = (6/d_B)[\varepsilon/(1 - \varepsilon)]$, given that $a' = 6\varepsilon/d_B$. For the very low voidages used here, $a' \cong a$. The only unknown is then $k_L a$, which is determined by minimizing the sum of the square of the difference between measured and predicted normalized concentration measurements. The standard regression solver in Excel was used. Concentration measurements were collected every 0.33 s and then every 10 data points were averaged and stored.

The results of a typical pulsed column with oxygen uptake experiment and mass transfer coefficient ($k_L a$) fit are shown in Figure 2. In Figure 2, the air flow rate is 1.04 mL/s with a 0.75 mm ID stainless steel nozzle (nozzle gas velocity 2.36 m/s), the cam amplitude is 1.36 mm, and the sealing rubber sheet is 3.18 mm thick. The value of $k_L a$ for the fit was 0.0008 s^{-1}.

Amplitude measurements

The natural gum rubber sheet at the base of the column is clamped between two stainless steel disks each 2.73 cm in diameter. The column cross-sectional area is 62.2 cm^2, which effectively allows motion of an area of 56.3 cm^2 of membrane. It is seen that the column is being forced with a flexible piston. As we learned, the rubber membrane acting as a piston sustained its own dynamics. At higher frequency, the movement of the membrane was not in phase with the motion of the disks to which they were affixed.

In this work amplitude was measured from center-to peak (half stroke), not trough-to-peak. We adjusted the amplitude of the metal disks to be 0.51 mm and used a 3.18 mm (1/8-in.) thick natural gum membrane as the mobile piston. The rubber sheet stretches to accommodate this forcing. By slowly turning the cam by hand and using the cathetometer to directly measure water column height change, A_0 (water amplitude as the frequency approaches 0) was determined as 0.303 mm. To determine actual liquid amplitudes (A^*) at various frequencies, a Styrofoam® disk was placed on top of the water and filmed as a function of frequency using a high-speed (1000 frame/s) digital camera (Kodak Ektapro Integer Model 1000HRC). This also helped to damp the standing surface waves that typically develop on the free surface of liquid in a harmonically excited container. It should be noted that the foam was water resistant so its small weight remained constant during the experiment and did not alter the mechanical behavior of the system. Tables

Table 1. Water Amplitudes from Styrofoam® Disk, Cam Setting 0.51 mm, and Three Thicknesses of Flexible Pistons at 0 Hz and A_0 = 0.303 mm

Cam Frequency (Hz)	Water A^* (mm)		
	1.59 mm (1/16-in.) Thick	3.18 mm (1/8-in.) Thick	6.35 mm (1/4-in.) Thick
10	0.38	0.23	0.38
15	0.92	0.52	0.31
17.5	**1.15**	0.84	0.46
20	0.61	**1.56**	0.61
22.5	0.38	0.91	0.92
25	0.31	0.39	**1.37**
30	0.31	0.13	0.46

Table 2. Water Amplitudes from Styrofoam® Disk, Cam Setting 1.36 mm, and Three Thicknesses of Flexible Pistons at 0 Hz and $A_0 = 0.74$ mm

Cam Frequency (Hz)	Water A^* (mm)		
	1.59 mm (1/16-in.) Thick	3.18 mm (1/8-in.) Thick	6.35 mm (1/4-in.) Thick
5	0.39	0.71	0.39
10	0.52	0.65	0.78
15	**1.69**	1.3	0.84
17.5	1.66	**2.46**	1.23
20	0.97	1.69	1.69
22.5	0.78	1.17	**1.94**
25	0.71	1.04	1.81
30	0.39	0.32	1.1

1 and 2 show the measured water amplitudes as a function of frequency for two different fixed cam settings of 0.51 mm (Table 1) and 1.36 mm (Table 2) and three different thicknesses of natural rubber used as the flexible piston. The Styrofoam® disk results were confirmed by introducing a very slow flow rate of bubbles into the column (0.05 mL/s) and digitally recording the bubble's relative position as a function of time and frequency, as it moves up the column.

Results and Discussion

In the following section, the effect of frequency on water amplitude was determined and results modeled as a spring and damper system. Induced bubble breakage at a low gas flow rate was analyzed using both a high-speed camera for visual observations and mass transfer experiments to gauge enhancement.

Amplitude

The results in Tables 1 and 2 show an amplitude maximum in frequency (highlighted in bold), which is a function of membrane thickness. An inertial viscoelastic model of the system was used to pinpoint the phase and magnitude differences between the pulsing membrane system and the responding water phase. The effect of membrane thickness (rigidity) was also deduced from such models. To simplify reporting our data, the cam amplitude setting will be used. When appropriate for discussion, the actual fluid amplitude (A^*) will be specified. For Tables 1 and 2, the water amplitude as the frequency approaches zero (A_0) was experimentally determined as 0.303 and 0.74 mm, respectively.

It is clear that the elastic nature of the membrane piston system introduces dynamics of the spring-inertia type. In the following section, we introduce models for the mechanical behavior of the piston. To study the dynamics between the vibrated flexible piston (rubber membrane) and the water phase above it, three different thicknesses of natural rubber were used for the flexible piston. Note, in the tables that the larger spring constants (thicker membranes) yield higher resonant frequencies (bold-faced numbers), as expected for a damped spring-inertia system.

Mechanical dynamic model for amplitude results: flexible piston

As an approximation, the membrane–water–cam system can be modeled as a second-order underdamped process with inertial viscoelastic behavior (IVE). Here the analogy is being made between the oscillating water column and the classic problem of the periodic forced oscillation of a body on a spring and damper. In the bubble column, the mass of the water is supported by the elastic membrane. The membrane itself is fixed at two locations: the wall and the piston driver. Thus, the elastic action of the membrane can be distributed as two springs with dampening: one spring for the action between the water and the driver piston and the second spring action between the water and fixed wall. The second-order differential equation for the system shown in Figure 3 is

$$M\frac{d^2s}{dt^2} + (\zeta_1 + \zeta_2)\frac{ds}{dt} + (k_1 + k_2)s = k_2 s_1(t) + \zeta_2\frac{ds_1}{dt} \quad (7)$$

In our case, where the excitation is a harmonic one, the displacement is $s_1 = s_0\sin(\omega t)$. The measured amplitude displacement using the foam cover is related to the excitation amplitude through geometrical considerations and conservation of volume, and can be seen to be

$$\frac{s_M(f)}{s_0} = \frac{s_{M0}}{s_0}\frac{k_2}{k_1 + k_2}\frac{\sqrt{1 + \frac{k_1 + k_2}{k_2}\left(2\xi_2\frac{f}{f_n}\right)^2}}{\sqrt{\left[1 - \left(\frac{f}{f_n}\right)^2\right]^2 + \left(2\xi\frac{f}{f_n}\right)^2}} = \frac{s_{M0}}{s_0}\frac{k_2}{k_1 + k_2}F(f) \quad (8)$$

where

$$\xi_2 = \frac{\zeta_2}{2\sqrt{k_2 M}} \qquad \xi = \frac{\zeta_1 + \zeta_2}{2\sqrt{(k_1 + k_2)M}} \qquad f_n = \frac{1}{2\pi}\sqrt{\frac{(k_1 + k_2)}{M}}$$

The frequency f_n is the undamped natural frequency of the system, ξ is the overall damping ratio, and ξ_2 is the second damping ratio. For the purpose of comparing with experimental results, the amplitude response function has been defined as the measured amplitude of the foam–liquid contact surface scaled by the cam amplitude setting. We note that the ratio s_{M0}/s_0 is a function of the geometry and is approximately a constant. Here

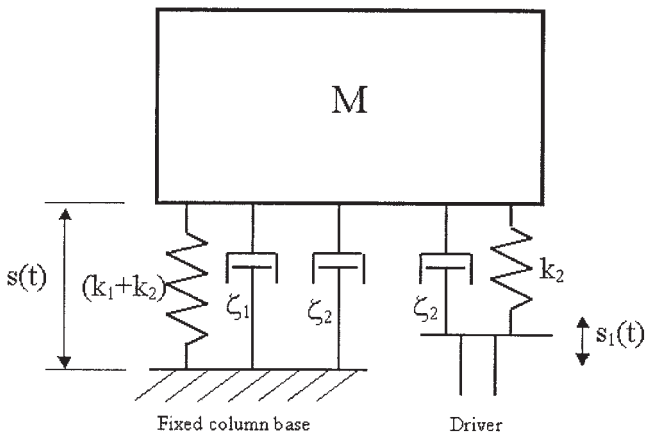

Figure 3. Dynamic model for forced bubble column.

s_0 is the cam amplitude setting. The rubber membrane and disk take the shape of the frustum of a cone when fully displaced, so the system gain (height of water displacement in column/height of cam displacement) is

$$\frac{s_{M0}}{s_0} = \frac{1}{3}\left[1 + \frac{r_2}{r_1} + \left(\frac{r_2}{r_1}\right)^2\right]$$

where r_1 is the column radius (=44.5 mm) and r_2 is the radius of clamping disk (=13.65 mm). Thus, $s_{M0}/s_0 = 0.467$.

We note in Eq. 8 that the limit as $f \to 0$ is

$$\frac{s_M(0)}{s_0} \to \frac{s_{M0}}{s_0}\left(\frac{k_2}{k_1 + k_2}\right)$$

Thus, results can be normalized by referring to this zero frequency limit, as we do later, by defining

$$A_0 = s_M(0) = s_0\left(\frac{s_{M0}}{s_0}\right)\left(\frac{k_2}{k_1 + k_2}\right)$$

Thus, the reduced form is

$$\frac{A^*(f)}{A_0} = F(f) = \frac{s_M(f)}{s_M(0)}$$

So,

$$A^* = s_0\left[\frac{s_M(f)}{s_0}\right] \qquad \text{and} \qquad A_0 = s_0\left[\frac{s_M(0)}{s_0}\right]$$

It is evident that this model reduces to the simple mass-spring-damper model when the damping coefficient ζ_2 approaches zero and the spring constant k_2 approaches infinity (perfectly stiff connection between the driving rod and the driven mass).

The measured foam–liquid amplitude from the experiment scaled by the cam amplitude setting is shown in Figure 4, together with the theoretical model prediction. The latter was obtained by fitting the data using the theoretical amplitude response function above. The error bars are indicative of the uncertainty interval of the amplitude measurement (at 95% confidence level). The fitted parameters together with the associated correlation coefficients for the fit are given in Table 3.

The overall damping coefficient is calculated from the fit constants, one of which is the undamped natural frequency. The resonance frequency f_{nd} is then calculated from the undamped natural frequency and the overall damping ratio. Because the overall damping ratio is very small in all cases (as expected, the system is subject to very little damping) the resonance frequency deviates very little from the undamped natural frequency. This would change if higher viscosity liquids are used. It should be noted that when looking at the system parameters (estimated by the curve fit of the theoretical model with the experiment), the uncertainty in the amplitude measurement is high enough to prevent any definite conclusions regarding the "universality" of the model. In any event, the model examined here is the simplest one that satisfactorily represents the data. This sort of model would also be applicable to the work of Krishna et al.,[19] where they used a simple loudspeaker to impart vibrations to the fluid phase. The resonance of the loudspeaker fabric has properties similar to those of the rubber membranes used in the present work.

Induced bubble breakup

After watching high-speed videos of the glass injector tube, we concluded the breakup of slugs in the injector tube is caused by oscillatory backflow. For example, when using low gas flow rates (0.18 mL/s, single injector) we observed large numbers of bubbles at very mild forcing (10–30 Hz), using a 3.18 mm (1/8-in.) thick natural gum rubber sheet, and at fixed cam amplitude settings of 1.36 and 0.51 mm (see Tables 1 and 2 for actual fluid amplitudes). The observed pattern in the column proper could be described as ideal bubbly flow. This result was entirely unexpected at these low frequencies and we are not aware of such phenomena reported in the literature. Two photographs (Figures 5a and 5b) show a rapid increase in the number of bubbles as the frequency is increased. In Figure 6, we show the actual bubble count for increasing frequency; the maximum occurs at nearly the same frequency as the resonance peak for the fluid amplitude shown in Table 3 ($\sim$18 Hz).

At an air flow rate of 0.18 mL/s (superficial nozzle gas velocity = 0.23 m/s) the single injector (1.0 mm ID) in the unforced BCR produced 10 bubbles/s. As shown in Figure 6, when forced at 17.5 Hz the number of bubbles increased to $>$500/s. Similar results were observed at other flow rates; for example, at a very low flow rate of 0.05 mL/s over 200 bubbles/s were produced at 17.5 Hz. This increase in bubble number (and consequently interfacial area) can be used to promote mass transfer (as detailed below), generate small bubbles in microscale reactor systems, and improve reaction rates, such as in fermentations and phase-transfer reactions. The number of bubbles/s was determined by two methods, both using a high-speed Kodak camera at 1000 frames/s (Kodak Ektapro Integer Model 1000HRC). As shown in the following section, we took pictures of bubbles leaving the injection nozzle, which allows direct bubble counting. In addition, cross sections of the column were recorded at varying distances above the injector. In this latter method, bubbles were grouped into size categories (10 diameter categories). Then the known volumetric flow rate is divided by the average bubble volume to determine the number of bubbles; this method is more approximate when compared with counting bubbles directly from the nozzle.

At all low flow rates tested (such as 0–15 mL/s injector) and oscillation frequencies used (such as 10–30 Hz), we observed no coalescence of the generated bubbles. We quantified this fact by visually counting bubbles at two cross-sectional locations above the oscillating membrane. The results at both 17.8 and 36.8 cm above the membrane were consistent and these were in agreement with the direct count made at the injector tip.

In a similar study, Krishna et al.[19] used a loudspeaker, as mentioned earlier, to force a single capillary BCR at a low gas nozzle velocity of 1.35 m/s (0.17 mL/s). Here bubble numbers show little increase from 0 to 100 Hz and steep local maxima approaching 120 bubbles/s near 100 and 125 Hz at amplitudes $>$ 2 mm. However, the forcing amplitudes portrayed by

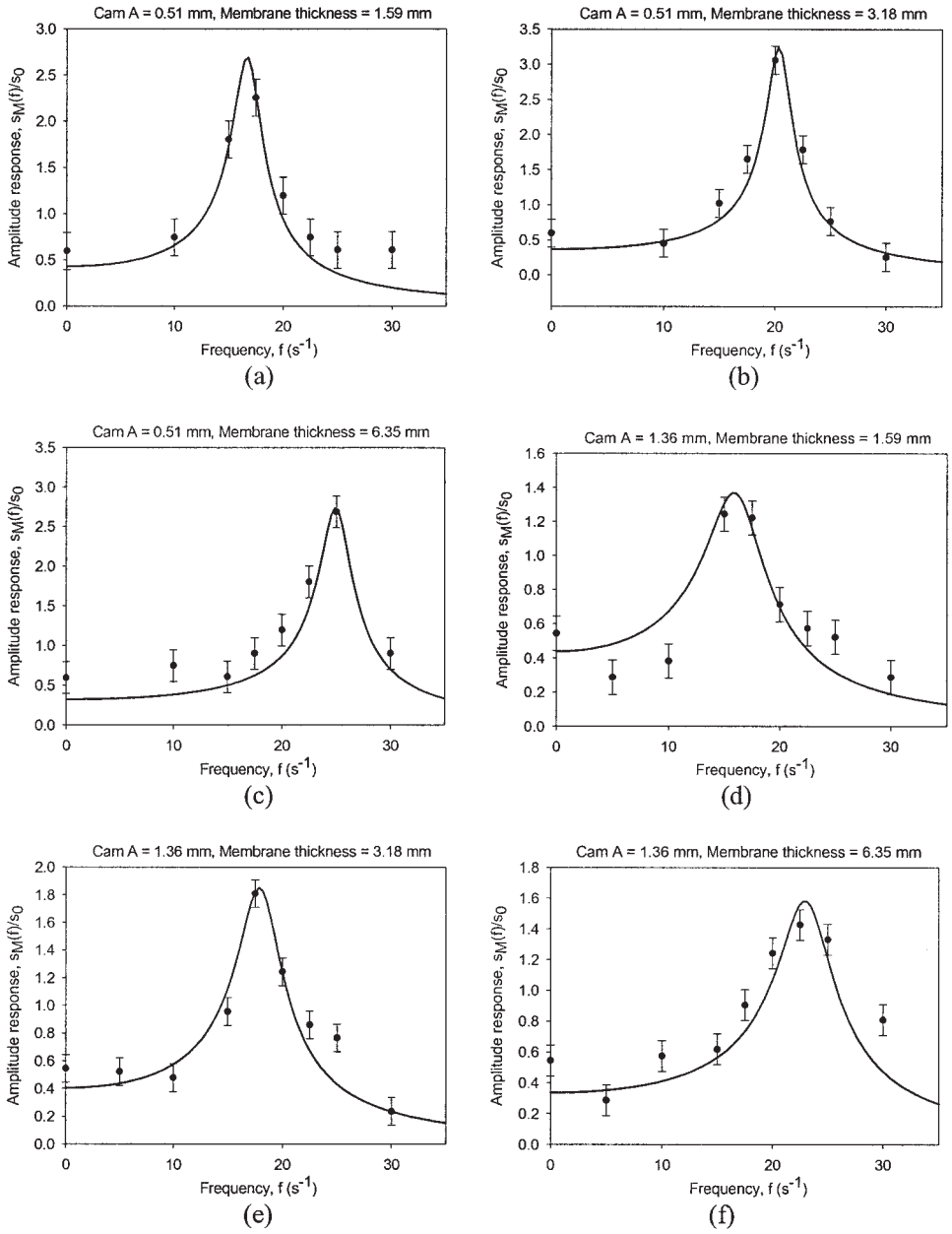

Figure 4. Styrofoam®–water interface amplitude measurements scaled by cam amplitude at various forcing frequencies.

Solid curve is fit of Eq. 8 with amplitude response $[s_m(f)/s_0]$.

Krishna et al.[19] seem unlikely from a loudspeaker system. For example, at 50 Hz, the indicated 6 mm amplitude on their 5.7 kg water column would require over 3000 Newtons of force. Later, Ellenberger and Krishna[20,24] used a solid piston base with electromagnetic vibration to force a single capillary BCR at a gas nozzle velocity of 0.83 m/s (0.528 mL/s) and amplitudes ranging from <0.01 to 0.32 mm. Results showed a linear increase in bubble number with frequency to the first maximum of about 125 bubbles/s again near 100 Hz. At these low flow rates our findings (Figure 6) show a much different result: the bubble frequency has reached a first maximum at 17.5 Hz with about 600 bubbles/s. Furthermore, our results show much greater bubble numbers at lower frequency for the first maximum, compared to those found by Krishna and Ellenberger. It is clear the elasticity of the rubber membrane, acting as a piston, has a unique effect on applied forcing. A "slingshot" effect arises as a consequence of the elastic membrane, giving rise to the well-known resonance attendant to a second-order damped-spring system of equations.

Photographs of column operation and induced bubble breakage

To come to grips with the curious breakage phenomenon, high-speed pictures using an all-glass air-injection system were taken. We performed initial studies to examine the effect of

Table 3. Dynamic Parameters of the Bubble-Column Mechanical Model

Cam amplitude (mm)	0.51	0.51	0.51	1.36	1.36	1.36
Membrane thickness (mm)	1.59	3.18	6.35	1.59	3.18	6.35
$\frac{s_{M0}}{s_0}\frac{k_2}{k_1+k_2}$	0.4284	0.3657	0.3215	0.4381	0.4014	0.3357
f_n (Hz)	16.8	20.4	25	16.3	18.1	23.2
$\left(\frac{2\xi}{f_n}\right)^2$ (1/Hz^2)	9.14E-05	3.10E-05	2.24E-05	4.11E-04	1.51E-04	8.71E-05
$\frac{k_1+k_2}{k_2}\left(\frac{2\xi_2}{f_n}\right)^2$ (1/Hz^2)	5.36E-05	2.71E-05	2.20E-05	1.50E-04	7.50E-05	5.81E-05
ξ	0.080	0.057	0.059	0.165	0.111	0.108
f_{nd} (Hz)	16.75	20.37	24.96	16.08	17.99	23.06
Correlation coefficient (%)	99.2	98.3	99.0	91.0	95.6	94.5

frequency, air flow rate, and amplitude. To date, the effect of frequency from 2.5 to 30 Hz at several air flow rates has been photographically studied. The pictures shown in Figure 7 were taken at 17.5 Hz vibration frequency with a gas feed rate of 0.18 mL/s and a cam amplitude setting of 1.36 mm. Here the actual water amplitude (found in Table 2) was measured to be 2.46 mm. The glass injector is 1.00 mm ID, with a vertical length of 38 mm. As shown in the pictures, gas is introduced from the left, whereas the right side of the tee is a dead leg simply used to help support the tee across the column.

The time span between consecutive pictures was 0.001 s. With an external vibration frequency set at 17.5 Hz, about 60 frames were captured for each vibration cycle. Approximately 30 pictures were taken in the upward movement of the membrane and the next 30 pictures were in the downward movement of each vibrating cycle. Shown in Figures 7a–7l, pictures taken every 0.005 s were chosen to show the entire process starting with the initial suck-back at time = 0, and the expulsion phase starting at time = 0.030 s.

Mechanism of low flow–induced breakage

The mechanisms and dynamics relevant to the induced bubble breakage observed in the forced bubble column at low flow rate conditions can be categorized as follows.

(1) *Discrete bubble formation and detachment at the injector tip*. This is typical of steady-state bubble injection in the nonjetting mode under low gas feeds and is controlled by surface tension, contact angle, buoyancy, and to a lesser extent virtual-mass inertia and gas discharge momentum. This mode of injection is also observed in the forced bubble column, but in an intermittent manner, especially when large gas plugs feed through the injector exit during the forcing cycle at modest instantaneous gas velocities (gas velocity at the injector exit varies substantially during the forcing cycle).

(2) *Liquid ingestion during the forcing cycle*. At low gas flow rates under unforced conditions liquid is ingested into the injector after individual bubbles leave the injector. This is a well-known capillary phenomenon, the effect of which declines with increasing pressure and gas flow rates and is also dependent on the acoustic impedance of the gas injection system. In the case of the forced column, this liquid ingestion is imposed rigorously by the oscillation of the liquid column. The amount of liquid ingested and the ingestion velocity are substantially larger under forcing. Their magnitudes depend on the amplitude of the oscillation of the liquid column, which depends on the mechanical "piston" amplitude (cam setting of the driver) and depends on frequency because the oscillation of the liquid column can be modeled as the response of a simple underdamped second-order system to harmonic excitation. The vigorous ingestion of liquid during the "downside" of the forcing cycle is of paramount importance for the generation of large numbers of small bubbles by the injector under forcing conditions. This will become apparent from the discussion of the ensuing phenomena.

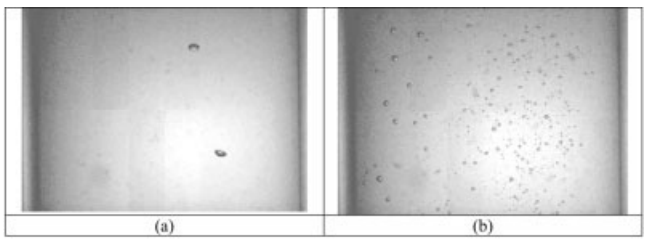

Figure 5. Photograph of column showing gas dispersion with and without oscillations.

(a) f = 0 Hz, membrane thickness = 3.18 mm, Q_g = 0.18 mL/s; (b) f = 17.5 Hz, cam amplitude = 1.36 mm, membrane thickness = 3.18 mm, Q_g = 0.18 mL/s.

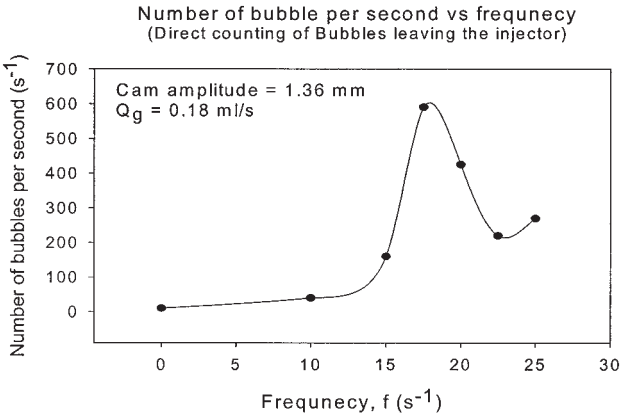

Figure 6. Number of bubbles generated at nozzle per second as a function of frequency.

Cam amplitude = 1.36 mm and Q_g = 0.18 mL/s (superficial nozzle gas velocity = 0.23 m/s).

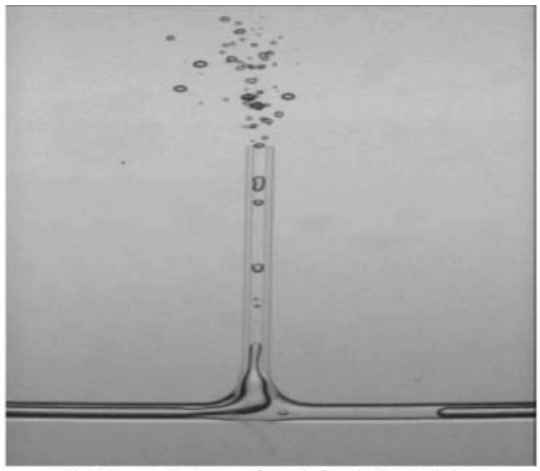

Fig 7a. t = 0 start of suck back (expulsion completed)

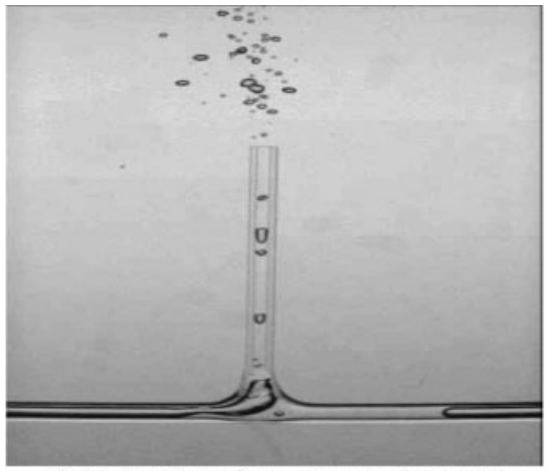

Fig 7b. t = 0.005s from start; note downward motion of the air bubbles in the injector

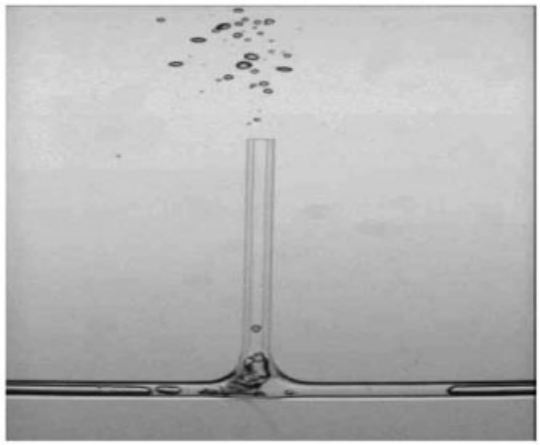

Fig 7c. t = 0.01s; continued downward movement of the bubbles

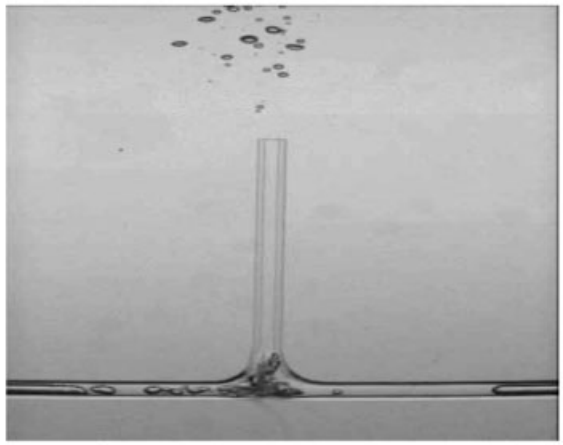

Fig 7d. t = 0.015s

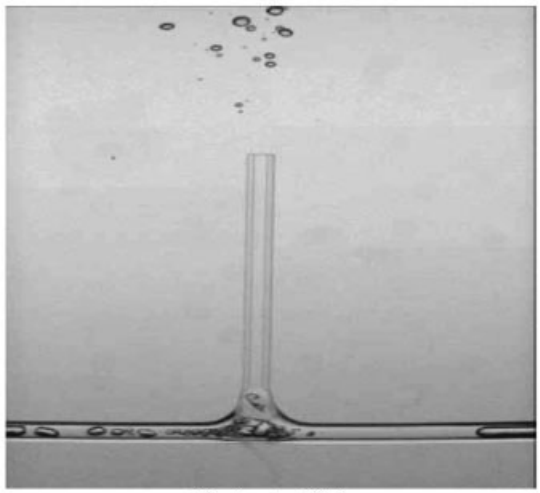

Fig 7e. t = 0.02s

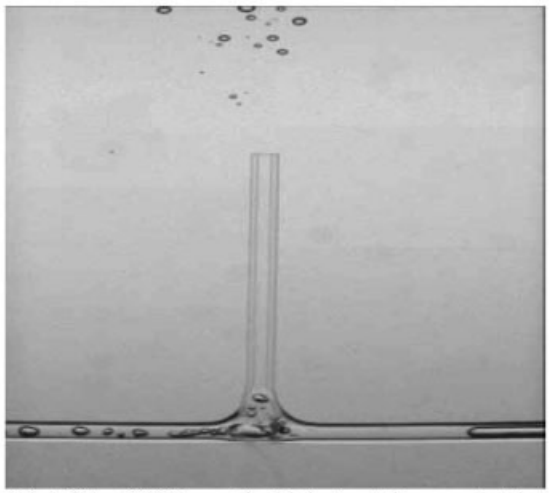

Fig 7f. t = 0.025s; vertical injector tube completely filled with water

Figure 7. Photographs of gas injector showing expulsion and suck-back phenomenon.

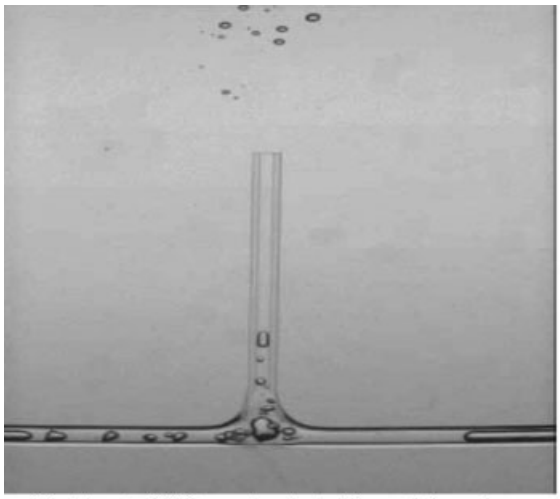

Fig 7g. t = 0.03s; note start of expulsion phase

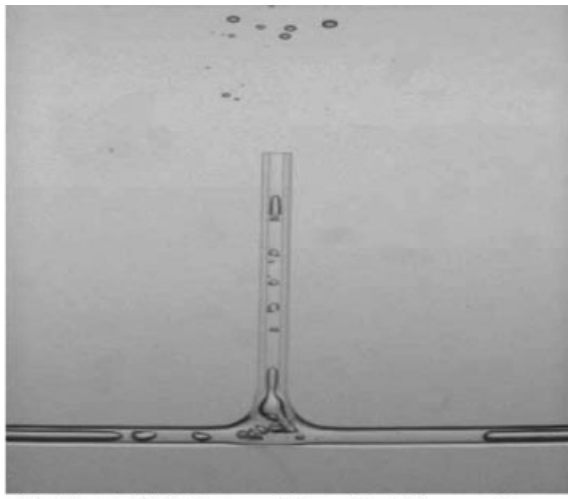

Fig 7h. t = 0.035s; expulsion of bubbles continues

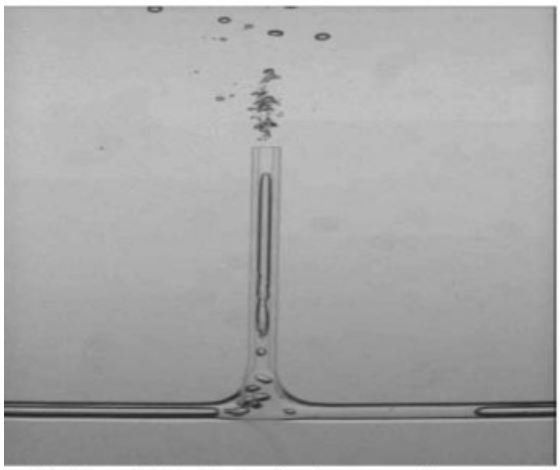

Fig 7i. t=0.04s; high velocity water slug causes additional bubble breakup at nozzle tip

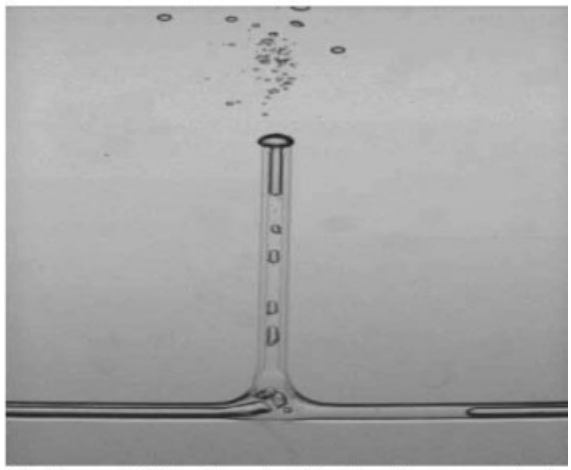

Fig 7j. t = 0.045s; large bubble forming at nozzle tip

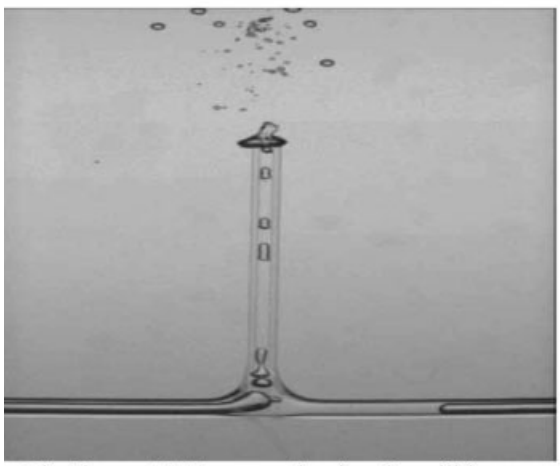

Fig 7k. t = 0.050; water slug in tube will impact bubble at ejector tip

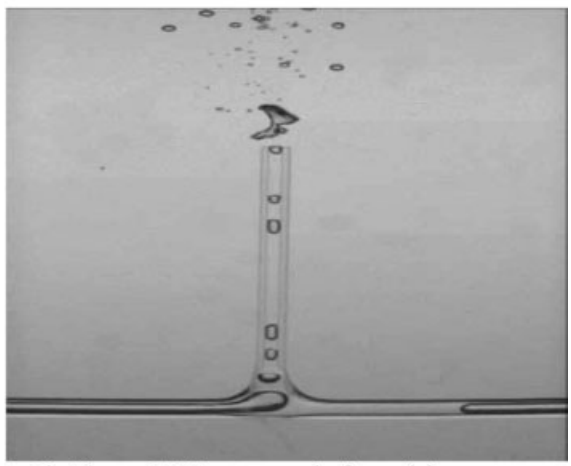

Fig 7l. t = 0.055s; near end of expulsion process

Figure 7. Continued.

(3) *Gas fragmentation and development of sustained two-phase flow inside the injector and injector feed line*. The ingested liquid in the injector (both in the straight vertical part and the horizontal part on either side of the "T" junction) forms a variety of two-phase flow regimes as it "mixes" with the gas in the injector. This "mixing" occurs both during the liquid ingestion part of the cycle as well as during the expulsion part of the cycle. The latter takes place during the "upswing" of the liquid oscillation in the column. This two-phase flow exists inside the injector throughout the cycle locally. This mixing results in the breakup of the gas phase into bubbles of a broad range of sizes, ranging from bubbles smaller than the injector tube inner diameter (1 mm), to Taylor-like gas plugs, all the way to very long gas plugs that can be viewed as a local form of annular flow. Often gas plugs and small bubble swarms coexist, giving the semblance of churn flow. Thus one can identify roughly three to four two-phase flow regimes: bubbly, slug/plug, churn, and annular. The two-phase flow in the injector is highly transient, thus these regimes are not in steady state and they are very localized. Apart from the instantaneous combination of gas and liquid superficial velocities, which traditionally influence the two-phase flow regime development, there are a few more phenomena that have been observed as contributing to the topology of the two-phase flow observed in the injector.

- During the ingestion part of the forcing cycle, small bubbles generated during the injection/expulsion part linger near the injector exit and are themselves ingested along with the liquid into the tube. These small bubbles linger near the exit of the injector because they have small rise velocities arising from buoyancy and are not able to survive the general downdraft in the liquid of the column. Larger bubbles that are partly inside the injector and partly outside at the point of reversal of the cycle are also fully ingested back into the injector tube.
- The "T" junction where the vertical part of the injector meets the horizontal also plays a significant role in breaking up gas bubbles and plugs with the aid of high-inertia liquid slugs. This occurs primarily during the liquid ingestion part of the cycle where gas plugs move down and are "smashed," as they decelerate against the horizontal wall of the "T," by the high-momentum liquid that follows them. Similar action is also observed during the injection part of the cycle as the gas plugs/bubbles are decelerated while moving from the horizontal to the vertical part of the injector. In this case the "dead" leg of the injector may act as a shock absorber depending on the amount of gas that happens to be in it.
- The transition of the two-phase flow from the horizontal to the vertical part may also play a role because the regime phase boundaries depend on tube orientation. This effect may not be significant given the small inner diameter of the tube, which diminishes the significance of gravitational effects.

(4) *Liquid-impact–induced breakup of large bubbles at the injector exit*. Here, we observe a very effective mechanism that produces large numbers of small bubbles during part of the forcing cycle. When a "large" bubble is injected it typically deforms by expanding outward, increasing its frontal area, thus increasing the drag on this emerging bubble, which is slowed down relative to the velocity of the gas that produces it. This slowdown is also aided by the fact that the gas bubble has substantially low inertia. Such bubbles that have been injected toward the end of the injection part of the cycle often cannot distance themselves enough from the injector exit during the ingestion part of the cycle and remain in the vicinity of the injector. When the injection begins again such bubbles are impacted by a high-momentum liquid jet, which often breaks them up in an explosive way. This type of breakup also occurs during the injection part of the cycle when the flow regime in the vertical part of the injector is slug/plug or churn. Under such circumstances a sizable but low-momentum gas bubble is injected, slowed down through increasing form-drag, and fragmented by the following high-momentum liquid slug that impacts it almost like a projectile.

If there is potential for resonance related to the injection system that can play a role in the suck-back process, which is responsible for the observed enhanced gas breakup, then this resonance should occur when the natural frequency of the oscillating liquid column approaches the acoustic frequency of the injection system. The relevant acoustic frequency is the one corresponding to the part of the injection system between the two high-impedance elements, that is, the needle valve and the gas–liquid interface at the injector end, which is moving inside the injector tube. For a first approximation, let us ignore the facts that (1) the fluid in the injector inside the column is a two-phase mixture, (2) there is an acoustic impedance change at the transition from the supply tube to the injection tube, and (3) the interface between the liquid in the injector and the gas in the supply line is moving very rapidly. An estimate of the associated natural acoustic frequencies of the gas part of the system based on the speed of sound and lengths between high-impedance elements (valve–gas/liquid interface) yields frequencies substantially higher than those used to pulse the column. This is so because the gas-filled lengths of tube between high-impedance elements are rather short. If assumption (2) is relaxed the associated frequencies become even higher. Consequently, the possibility of a serious effect of the injection system used during the experiments on the performance of the injection and the phenomena related to the generation of large numbers of small bubbles is small. Because this assessment was based on an oversimplified view of the injector internal dynamics, we tested this conclusion during the experiments by changing the location of the upstream high-impedance element. This was done by placing a porous plug (frit) on the feed line at the point where this line enters the column and downstream of the flow-regulating needle valve. The volume from the frit to the injector tip was 0.773 mL, which is about a 50% reduction compared to the volume from the needle valve to the injector tip. We found that no observable/measurable difference in performance existed between the two configurations.

The generation of large numbers of small bubbles in the forced bubble column under low gas flow rates occurs primarily because of the breakup of the gas phase in the two-phase flow forming in the injector as a result of liquid ingestion. The mechanisms described under (3) and (4) above are very significant for this process. Overall effectiveness of bubble generation depends heavily on injector design, gas flow rate and amplitude, and, to a lesser degree, frequency. If the air plenum is free of restrictions and designed for gas compression and expansion then suck-back and expulsion can be rigorously imposed. However, in the limit, if a large impendance is placed at the injector outlet (such as a frit), the suck-back will be lessened and perhaps eliminated, and the observed enhancements asymptotically disappear.

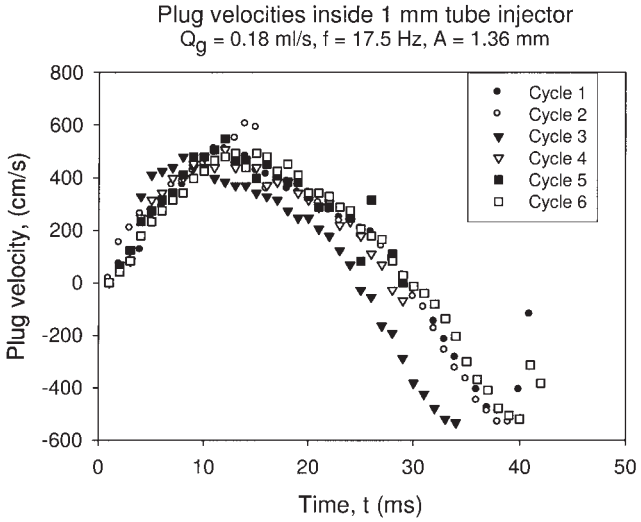

Figure 8. Plug velocity as a function of time during different cycles.

Injector ID = 1 mm, f = 17.5 Hz, cam amplitude = 1.36 mm, Q_g = 0.18 mL/s.

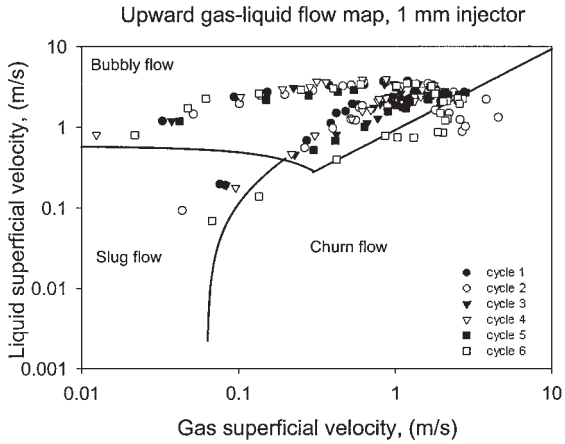

Figure 10. Flow regime map for upward gas–liquid flow inside the injector along with flow regime transition lines.

Injector ID = 1 mm, f = 17.5 Hz, cam amplitude = 1.36 mm, Q_g = 0.18 mL/s.

Correlation of induced bubble breakage

Using the high-speed photographs, we were able to determine the instantaneous velocities of air/water plugs and the instantaneous void fractions in the vertical portion of the injector, during both the suck-back and the expulsion phase. These results (for six cycles) are plotted in Figures 8 and 9. Here the glass tube ID was 1.0 mm, the air flow rate was 0.18 mL/s, the forcing frequency was 17.5 Hz, and the cam amplitude was 1.36 mm (2.46 mm actual water amplitude; see Table 2).

There are two important features from these figures. First Figure 8 shows that velocities approaching 600 cm/s are possible both during the suck-back and expulsion portion of the cycle. Figure 9 shows that the void fraction (gas volume/total volume) in the vertical portion of the injector is never 1.0; in other words, water was always present in the injector during both suck-back and expulsion.

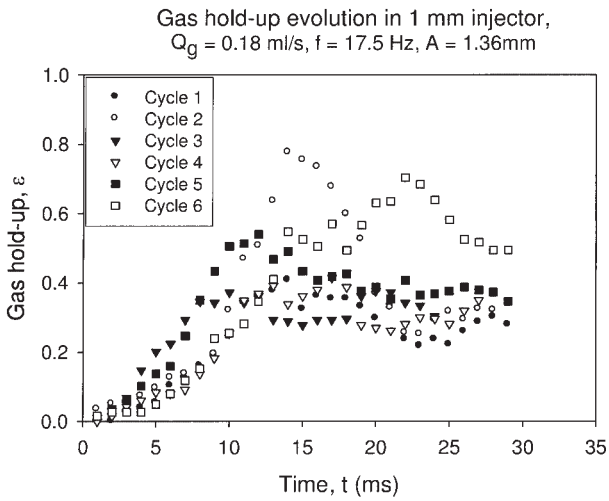

Figure 9. Gas holdup inside injector as a function of time.

Injector ID = 1 mm, f = 17.5 Hz, cam amplitude = 1.36 mm, Q_g = 0.18 mL/s.

It is possible to plot the data from Figures 8 and 9 onto a gas–liquid flow field map. This is done in Figure 10 following Taitel et al.[25] for tubes with ID $\ll$ 5 cm. The transition lines in Figure 10 are based on steady-state flow conditions. The suck-back and expulsion process is far too rapid to allow for steady-state conditions, in the traditional sense. However, Figure 10 indicates a flow transition from bubbly to churn to slug flow during the expulsion cycle, which was also experimentally observed. For example, Figure 7h indicates bubbly flow; Figure 7i may indicate churn flow (although the resolution may not be sufficient); and Figure 7j shows slug flow. For a more detailed description of these flow transitions see Triplett et al.[26] and Wallis.[27] The results in Figure 10 have important implications for systems where gas and liquid mixing in microchannels is important. Work is currently in progress to apply this technology to microreactors.

Mass transfer measurements for induced bubble breakage

We performed experiments to measure the effect of vibration frequency, amplitude, and gas flow rate on the volumetric mass- transfer coefficient. For these experiments, a single stainless steel injector (ID = 0.75 mm; vertical length = 38 mm) was used. The liquid height for all experiments was maintained at 82 cm.

In Figure 11a we have plotted k_La^* (the asterisk denotes the vibrated case) as a function of frequency for three air flow rates [0.51, 1.04, 2.0 mL/s or equivalent nozzle superficial gas velocity (SGV) 1.15, 2.36, 4.53 m/s] and a cam amplitude of 1.36 mm using a 3.18 mm thick membrane. This figure shows that a cam amplitude setting of 1.36 mm gives increasing k_La^* values with increasing flow rate, over the flow rate range tested. The k_La^* enhancement can be significant. For example, with a flow rate of 2 mL/s and 17.5 Hz forcing, enhancement of 100%

is seen in Figure 11b where the vibrated case (k_La^*) is divided by the unvibrated case (k_La).

There is some agreement between the normalized mass-transfer trends in Figure 11b and the membrane amplitude response shown in Figure 4e. Notice that the maximum recorded k_La^* value at 17.5 Hz corresponds satisfactorily to the membrane resonant frequency (maximum expected amplitude) 17.99 Hz. This result is also found in Figure 12, where the k_La^* behavior at 2.0 mL/s is plotted for the 6.35 mm thick membrane (here, also, for comparison, the results for the 3.18 mm thick membrane are plotted). The maximum in Figure 12 at 22.5 Hz is in agreement with Figure 4f, where the membrane resonant frequency is shown at 22.76 Hz. However, over the range of frequencies and low flow rates studied, the enhancement of k_La^*/k_La does not correlate well with enhancement in liquid amplitude. In other words, $(k_La^*/k_La)/(A^*/A_0) \neq 1$ at low gas velocities. It is clear that a small amount of intense mass transfer occurred in the injection tube, but the residence time was quite small, so the overall contribution was negligible.

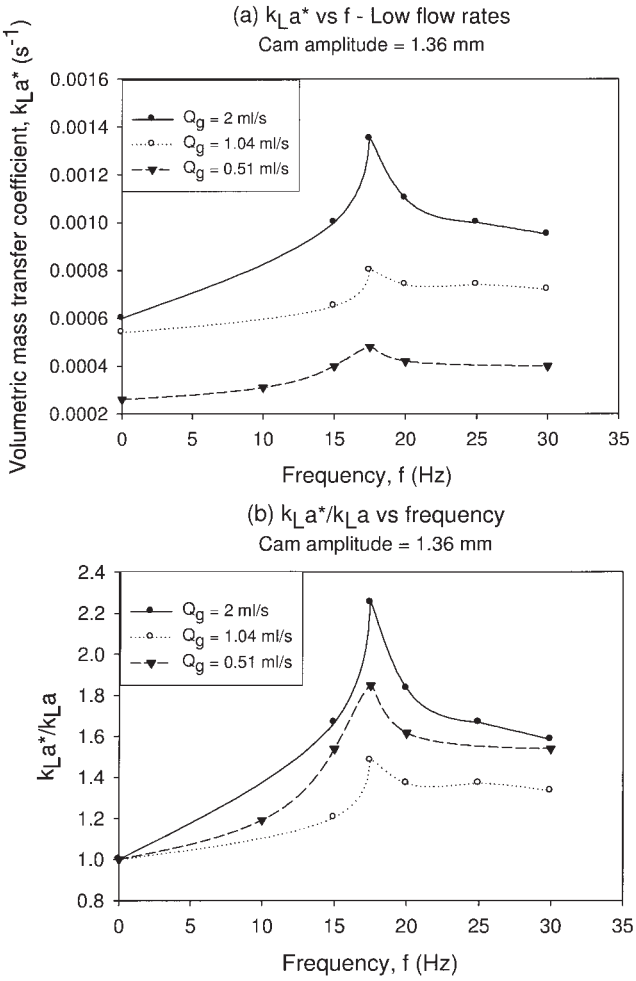

Figure 11. Volumetric mass-transfer coefficient as a function of frequency for three different gas flow rates.

(a) Absolute k_La^*; (b) ratio of vibrated to nonvibrated case, k_La^*/k_La.

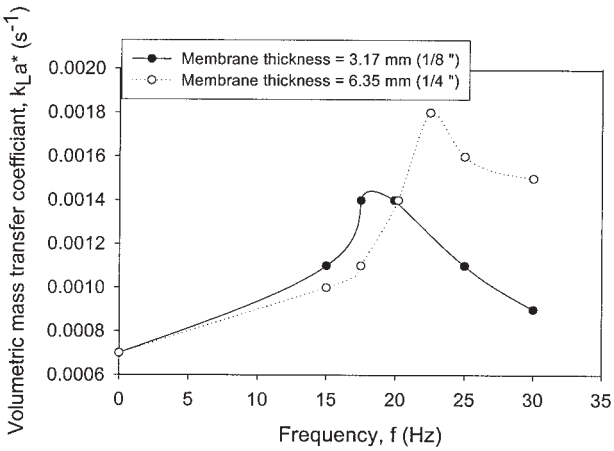

Figure 12. Effect of membrane thickness on volumetric mass-transfer coefficient as a function of frequency.

Cam amplitude = 1.36 mm, Q_g = 2.0 mL/s.

Conclusions

Experiments have indicated that optimum operation of the forced bubble column, in terms of the maximization of the number of small bubbles produced and minimization of their size under fixed low gas flow rates, occurs as a function of both frequency and amplitude. The best frequency is associated with the resonance based on the mechanical performance of the forcing system. This was confirmed through experiments by varying the stiffness values of the elastic membrane. These experiments demonstrated that the optimum operating frequency is associated with maximum amplitude of the oscillatory motion of the column liquid and can be manipulated by changing the elasticity of the forcing membrane piston. Higher stiffness produced higher resonant frequencies, which were associated with optimum bubble column performance. Thus, the optimum performance of the column at low gas flow rates depends on tuning the frequency to a resonant mode that yields the largest fluid amplitude. Other conclusions of these experiments are that the wave motion of the bubble column's free surface, which is quite violent at resonant conditions, does not play any apparent role in influencing the injection process. This was documented by observing the injection process and the entire bubble column with the foam cover in place and without the cover. No visible difference was observed.

The complete mechanism for bubble breakup inside the injector is complex and periodic. Apart from the slug flow regime, bubbly flow and local annular flow were also observed. Flow inside the injector is highly transient and can undergo continuous regime transitions. Gas bubbles break up inside the injector in a broad range of sizes from individual bubbles less than the tube diameter to elongated Taylor-like plugs. Also, we observed during the liquid-ingestion part of the cycle that small bubbles are ingested from the neighborhood of the injector tip. The tee junction of the injector (where the vertical part of the injector meets the horizontal) allows high-momentum liquid to have an impact on gas bubbles and slugs, further promoting breakage. During the expulsion cycle, the impact of high-momentum liquid slugs from the gas feeder tube helps break up gas slugs/bubbles at or near the injector tip, an impact that can

dramatically increase bubble numbers. It is obvious that several modes of breakage were operating in the present experiments, a clear case of serendipity.

Notation

a = gas–liquid interfacial area per unit volume of liquid, cm^2/cm^3
a' = gas–liquid interfacial area per unit volume of dispersion, cm^2/cm^3
A_0 = water amplitude as frequency approaches zero, mm
A^* = water amplitude at particular forcing frequency for flexible piston, mm
A_c = column cross-sectional area, cm^2
C = oxygen concentration, $gmol/cm^3$
C_0 = initial oxygen concentration, $gmol/cm^3$
C^* = oxygen saturation concentration, $gmol/cm^3$
f = frequency, Hz
f_n = undamped natural frequency, Hz
f_{nd} = resonance frequency, Hz
k_L = liquid-phase mass transfer coefficient, cm/s
k_La = liquid-phase volumetric mass-transfer coefficient, s^{-1}
k_La^* = liquid-phase volumetric mass-transfer coefficient, vibrated case, s^{-1}
k_1 = spring constant aligned with the water and fixed wall, g/s^2
k_2 = spring constant aligned with the membrane, g/s^2
M = mass of the system, g
Q_g = gas volumetric flow rate, cm^3/s
R = rate of oxygen transfer, gmol/s
$s(t)$ = displacement of water as a function of time, mm
s_0 = height of cam displacement, mm
$s_1(t)$ = cam displacement as a function of time = $s_0\sin(\omega t)$, mm
$s_M(f)$ = water amplitude as a function of frequency, mm
s_{M0}/s_0 = gain for model system in Eq. 8 = (height of water displacement in column/height of cam displacement), dimensionless
t = time, s
Δz = differential height of column, cm

Greek letters

ε = gas holdup, dimensionless
ε^* = gas holdup vibrated case, dimensionless
ζ_1 = damping coefficient aligned with the water and fixed wall, g/s
ζ_2 = damping coefficient aligned with the membrane, g/s

Literature Cited

1. Santhanam V, Knopf FC, Acharya S, Gutmark E. Fluorescence and temperature measurements in a actively forced swirl-stabilized spray combustor. *J Propul Power.* 2002;18:855-865.
2. Bretsznajder S, Pasiuk W. Absorption in a pulsed column. *Int Chem Eng.* 1964;4:61-66.
3. Bretsznajder S, Lesniewicz L, Pasiuk W. *Bull Acad Polon Sci Ser Sci Chim Geol Geogr.* 1959;7:591.
4. Harbaum KL, Houghton G. Effects of sonic vibrations on the rate of absorption of gases from bubble beds. *Chem Eng Sci.* 1960;13:90-92.
5. Harbaum KL, Houghton G. Effects of sonic vibrations on the rate of absorption of carbon dioxide in gas bubble-beds. *J Appl Chem.* 1962; 12:234-240.
6. Baird MHI. Sonic resonance of bubble dispersions. *Chem Eng Sci.* 1963a;18:685-687.
7. Baird MHI. Vibrations and pulsations: Bane or blessing? *Br Chem Eng.* 1966;11:20-25.
8. Baird MHI, Garstang JH. Gas absorption in a pulsed bubble column. *Chem Eng Sci.* 1972;27:823-833.
9. Bartsch A. Acceleration of mass transfer in gas–liquid reactions by sonic vibrations—Fat hydrogenation as a test reaction. *Z Naturforsch.* 1995;50:228-234.
10. Krishna R, Ellenberger J. Improving gas–liquid mass transfer in bubble columns by applying low-frequency vibrations. *Chem Eng Technol.* 2002a;25:159-162.
11. Krishna R, Ellenberger J. Improving gas–liquid contacting in bubble columns by vibration excitement. *Int J Multiphase Flow.* 2002b;28: 1223-1234.
12. Baird MHI. Resonant bubbles in a vertically vibrating liquid column. *Can J Chem Eng.* 1963b;4:52-55.
13. Jameson GJ. The motion of a bubble in a vertically oscillating viscous liquid. *Chem Eng Sci.* 1966;21:35-48.
14. Jameson GJ, Davidson JF. The motion of a bubble in a vertically oscillating liquid: Theory for an inviscid liquid, and experimental results. *Chem Eng Sci.* 1966;21:29-34.
15. Leighton TG, Wilkinson M, Walton AJ, Field JE. Studies of non-linear bubble oscillations in a simulated acoustic field. *Eur J Phys.* 1990;11: 352-358.
16. Ellenberger J, van Baten JM, Krishna R. Intensification of bubble columns by vibration excitement. *Catal Today.* 2003;79/80:181-188. [Also see website ct-cr4.chem.uva.nl/sonicsim/]
17. Fawkner RD, Kluth PP, Dennis JS, Bubble formation at orifices in pulsed, flowing liquids. *Trans IChemE.* 1990;68A:69-73.
18. Grinis L, Monin Y. Influence of vibrations on gas bubble formation in liquids. *Chem Eng Technol.* 1999;22:439-442.
19. Krishna R, Ellenberger J, Urseanu MI, Keil FJ. Utilization of bubble resonance phenomena to improve gas–liquid contact. *Naturwissenschaften.* 2000;87:455-459.
20. Krishna R, Ellenberger J. Influence of low-frequency vibrations on bubble and drop sizes formed at a single orifice. *Chem Eng Process.* 2003;42:15-21.
21. Yang GQ, Luo X, Lau R, Fan LS. Bubble formation in high pressure liquid–solid suspensions with plenum pressure fluctuations. *AIChE J.* 2000;46:2162-2174.
22. Ma J. *Forced Bubble Columns.* MS Thesis. Baton Rouge, LA: Louisiana State University; 2003.
23. Rice RG, Do DD. *Applied Mathematics and Modeling for Chemical Engineers.* 1st Edition. New York, NY: Wiley; 1995.
24. Ellenberger J, Krishna R. Improving mass transfer in gas–liquid dispersions by vibration excitement. *Chem Eng Sci.* 2002;57:4809-4815.
25. Taitel Y, Bornea D, Dukler AE. Modeling flow pattern transitions for steady upward gas–liquid flow in vertical tubes. *AIChE J.* 1980;26: 345-354.
26. Triplett KA, Ghiaasiaan SM, Abdel-Khalik SI, Sadowski DL. Gas–liquid two-phase flow in microchannels. Part I: Two-phase flow patterns. *Int J Multiphase Flow.* 1999;25:377-394.
27. Wallis GB. *One-Dimensional Two-Phase Flow*. 1st Edition. New York, NY: McGraw-Hill; 1969.

Manuscript received Feb. 11, 2005, and revision received Aug. 26, 2005.